

# EFFECT OF INTERACTION OF FLAPPING HYDROFOIL MOTION PARAMETERS ON THRUST PULSATION PERFORMANCE

Reference NO. IJME 1202, DOI: 10.5750/ijme.v165iA2.1202

Q Y Cao, L X Hou\*, Z X Wang, X Chang, L L Yin, N Gao, W G Chen, and J Q Zhu, Dalian Maritime University, China

\* Corresponding author. L X Hou (Email) houlixun@dlnu.edu.cn

KEY DATES: Submission date: 14.07.2022 / Final acceptance date: 24.08.2023 / Published date: 27.11.2023

## SUMMARY

This study presents a novel index to assess the thrust propulsion performance of flapping-hydrofoil, and identifies the order of priority of motion parameters that affect the thrust pulsation amplitude. The flapping motion is simulated using the Udf (user-defined motion) feature in the commercial software Fluent, and the impacts of three flapping motion parameters on flapping thrust are investigated by manipulating these parameters. The results of the numerical simulation indicate that there is a positive correlation between the heave amplitude and the thrust pulsation amplitude. Additionally, the thrust pulsation amplitude is interactively affected by the pitch amplitude, the phase difference between horizontal and heave motion, and the heave amplitude. The Levenberg-Marquardt Algorithm is employed to fit the function that relates the thrust pulsation amplitude with the three motion parameters. The coefficients obtained from the fitting function indicate the impacts of the interaction effect, as well as the effect of each motion parameter on the pulsation amplitude.

## KEYWORDS

Flapping hydrofoil, Propulsion performance, Interaction effect, Hydrodynamic performance, Levenberg-Marquardt algorithm

## NOMENCLATURE

$\theta_0$	Pitch amplitude( $^\circ$ )
$\omega(\omega=2\pi f)$	Circular frequency
$\psi$	Pitch and heave phase difference
$\varphi$	Surge and heave phase difference
$\theta(t)$	Transient rotation angle( $^\circ$ )
$\rho$	Flow density
$x_{(t)}$	Transient horizontal displacement
$h_{(t)}$	Transient vertical displacement
$p$	Pressure
$x_0$	Heave amplitude
$h_0$	Vertical amplitude
$t$	time
$C_t$	Thrust coefficient
$C_l$	Lift coefficient
$C_m$	Moment coefficient
$P_a$	Thrust coefficient pulsation amplitude

tests to investigate the impact of pitch angle of flapping hydrofoil motion and Strouhal number on propulsion performance, based on single-Dof and two-Dof motions. The study concluded that decreasing the pitch angle resulted in a higher average thrust and improved propulsion efficiency for higher Strouhal numbers. Ashraf et al. [3] conducted a study on the effects of airfoil thickness and curvature on propulsion performance at different Reynolds numbers for various airfoil types. The results indicated that as the Reynolds number increased, the thicker airfoils contributed to a better propulsion performance. The leading-edge vortices were identified as playing a crucial role in flapping hydrofoil propulsion. The study conducted by Read et al. [4] investigated the phase difference between pitching motion and heave motion, as well as the influence of Strouhal number on propulsion performance. The findings indicated that the optimal propulsion efficiency of 50%~60% was achieved when the phase difference between pitching motion and heave motion was in the range of  $90^\circ$ ~ $100^\circ$ . Yu et al. [5] conducted numerical simulations to investigate the effects of frequency, heave amplitude, and pitch amplitude on propulsion performance. The findings revealed that the propulsion efficiency of the flapping hydrofoil was improved with higher frequency and heave motion amplitude. Moreover, the low-efficiency zone vanished with an increase in pitch amplitude. Zhang et al. [6] studied the effect of flapping frequency, amplitude, and phase angle on the thrust of a NACA0012 airfoil. The results revealed that the thrust generated by the airfoil increased with the increase of flapping frequency or amplitude, and that the phase angle had little effect on

## 1. INTRODUCTION

In recent years, there has been considerable research interest in the development of underwater vehicles. Inspired by the natural ability of aquatic creatures to generate thrust and lift through wing turbulence, some scholars have explored the use of this characteristic in the development of thrusters for underwater vehicles [1].

Researchers typically use either experimental or numerical simulation methods to investigate the performances of flapping hydrofoil. Techet et al. [2] conducted water tunnel

the thrust. Zhao et al. [7] focused on the fluid-structure interaction (FSI) and energy extraction performance of a novel flapping-foil based flow-energy harvester. They discovered that the thrust generated by the foil increased with the increase of heave amplitude, while the energy efficiency of the foil decreased with the increase of pitch amplitude.

In contrast to previous studies on 2-Dof motion, Esfahani et al. [8] found that incorporating horizontal motion to modify the effective angle of attack and changing the shedding mode of hydrofoil trailing edge vortex and wake surface could improve the propulsion performance. This discovery has inspired the development of various forms of motion trajectories. Yang et al. [9] proposed the “8” shaped motion trajectory and suggested that increasing horizontal reciprocating motion can generate multiple vortices, which are conducive to improving thrust. Zhang et al. [10] proposed the “∞” shaped motion trajectory, arguing that it had the advantages of multiple thrust peaks, average thrust, and high propulsion efficiency. Chen et al. [11] proposed the elliptical motion trajectory and studied the effects of the ratio of heave amplitude to horizontal motion amplitude on propulsion performance, concluding that a ratio of 2 is beneficial to improving the propulsion performance of flapping hydrofoils.

This study introduces a new parameter, the pulsation amplitude of thrust, to evaluate the propulsion performance of a flapping hydrofoil. Three motion parameters – heave amplitude, pitch amplitude, and phase difference between heave and a horizontal motion – are analysed for their impacts on the pulsation amplitude of thrust. The relationship between these motion parameters and the thrust pulsation amplitude is determined using the Levenberg-Marquardt optimization algorithm and the weight coefficient is used to reflect the influence of these three motion parameters on the thrust pulsation amplitude. This work provides a comprehensive evaluation of the flapping hydrofoil’s propulsion performance.

## 2. METHOD

### 2.1 FLAPPING MOTION MODEL

In this study, the flapping hydrofoil’s motion is composed of pitch motion, heave motion, and horizontal reciprocating motion. The motion equations under different degrees of freedom are as follows (1)-(3):

$$x_{(t)} = x_0 \sin(\omega t + \varphi) \quad (1)$$

$$h_{(t)} = h_0 \sin(\omega t) \quad (2)$$

$$\theta_{(t)} = \theta_0 \sin(\omega t + \psi) \quad (3)$$

Equations (1)-(3) are displacement equations of horizontal reciprocating motion, heave motion and pitching motion respectively. Its sub-motion motion mode is shown in Figure 1:

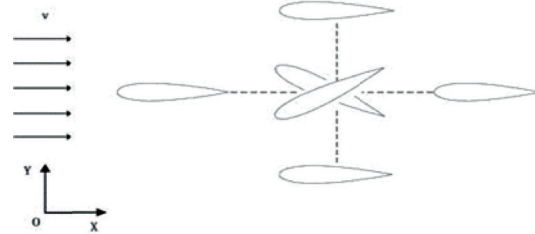


Figure 1. Flapping hydrofoil motion mode

According to the experiments and numerical simulation settings of Read [3] and Chen [11], a two-dimensional NACA0012 airfoil is selected, and the chord length  $c$  is 0.1m, the pitch axis is set as 1/3 of the airfoil, the ratio of heave to horizontal motion amplitude is 2, the frequency  $f$  is 0.8Hz, the pitch amplitude and heave motion phase difference  $\psi$  is  $90^\circ$ . The phase difference between heave and horizontal motion is set as  $\varphi = 60^\circ \sim 120^\circ$ . According to the research of Qing [12], the pitching amplitude range is  $\theta_0 = 10^\circ \sim 30^\circ$ . To achieve the speed of underwater vehicle, a Reynolds number of  $Re = 40000$  has been set, and the design of the numerical simulation variable group is presented in Table 1.

Table 1. Numerical simulation variable group

Parameters	Parametric design
$h_0$	$0.5c, 0.625c, 0.75c, 0.875c, c$
$\theta_0$	$10^\circ, 15^\circ, 20^\circ, 25^\circ, 30^\circ$
$\varphi$	$60^\circ, 75^\circ, 90^\circ, 105^\circ, 120^\circ$

The motion track diagram of this numerical simulation study has been determined based on the settings of different motion parameters, as depicted in Figure 2.

### 2.2 NUMERICAL METHOD AND MESH GENERATION

In this study, the hydrodynamic performance of the flapping hydrofoil of the NACA0012 airfoil is calculated based on the two-dimensional Navier-Stokes equation. Based on the findings of Young’s study [13], the calculation control equation for the viscous fluid model is expressed as follows:

$$\rho \left( \frac{\partial u}{\partial t} + u \frac{\partial u}{\partial x} + v \frac{\partial u}{\partial y} \right) = \mu \left( \frac{\partial^2 u}{\partial x^2} + \frac{\partial^2 u}{\partial y^2} \right) - \frac{\partial p}{\partial x} \quad (4)$$

$$\rho \left( \frac{\partial u}{\partial t} + u \frac{\partial u}{\partial x} + v \frac{\partial u}{\partial y} \right) = \mu \left( \frac{\partial^2 u}{\partial x^2} + \frac{\partial^2 u}{\partial y^2} \right) - \frac{\partial p}{\partial y} \quad (5)$$

The surface forces obtained through calculations are expressed in dimensionless:

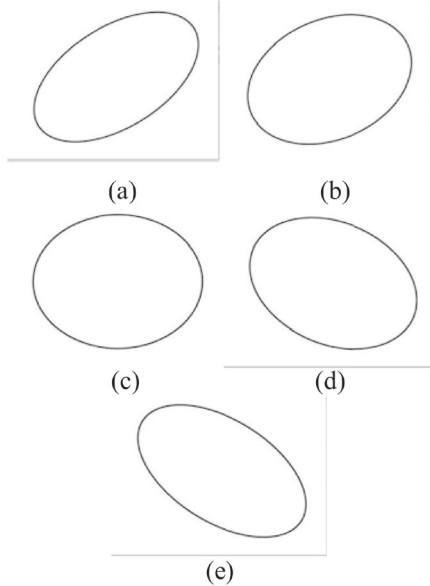


Figure 2. Motion trajectories for different motion parameters (a)  $\varphi = 60^\circ$  (b)  $\varphi = 75^\circ$  (c)  $\varphi = 90^\circ$  (d)  $\varphi = 105^\circ$  (e)  $\varphi = 120^\circ$

$$C_t = \frac{F_x(t)}{0.5 \rho v^2 c} \quad (6)$$

$$C_l = \frac{F_y(t)}{0.5 \rho v^2 c} \quad (7)$$

$$C_m = \frac{M(t)}{0.5 \rho v^2 c} \quad (8)$$

The thrust coefficient pulsation amplitude is defined as:

$$P_a = C_{t,max} - C_{t,min} \quad (9)$$

The two-dimensional numerical simulations are carried out based on the commercial software Fluent. The SST  $k-\omega$  turbulence model [1] is selected, the second-order upwind is adopted to ensure the accuracy of calculation, and the SIMPLEC model is adopted for pressure-velocity coupling. The flapping hydrofoil motion trajectory is defined through the user-defined Function (Udf), and the Fluent self-driving grid technology is utilized to accomplish mesh updating and reconstruction. The size of the computing domain is set to  $80c \times 40c$ , and the  $12c \times 10c$  grid encryption area is set to accurately capture of the movement within the region, as shown in Figure 3:

The unstructured mesh technology of ANSYS built-in mesh module is used for grid division. The dynamic grid model is adopted to realize the simulation of the flow field shape in the boundary motion. The boundary motion

law is determined by the custom function. The boundary motion form is determined by the calculation results of the previous step, and the flow field grid is updated according to the iteration of the previous step. In order to ensure the calculation accuracy, the maximum iteration of the update grid is set to 100 times, the minimum dynamic grid size is slightly less than the height of the first layer of the boundary layer. The accuracy of the calculation results is controlled and the residual is set to  $1e-05$ .

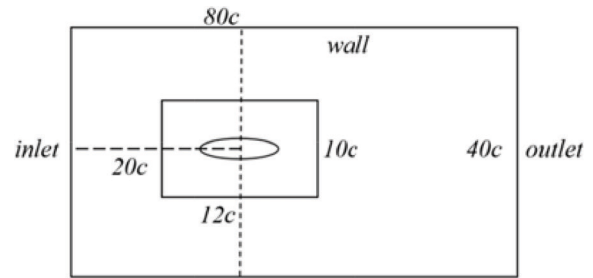


Figure 3. Schematic diagram of the computational domain

Different turbulence models have different  $y^+$  value requirements, which determines the height of the first layer mesh. For the SST  $k-\omega$  model, a  $y^+$  of 1 is necessary to ensure that the first layer mesh is in the sticky bottom layer to ensure the calculation accuracy. Therefore, the height of the first boundary layer complies with the  $y^+ = 1$  standard. The mesh generated for simulations is shown in Figure 4.

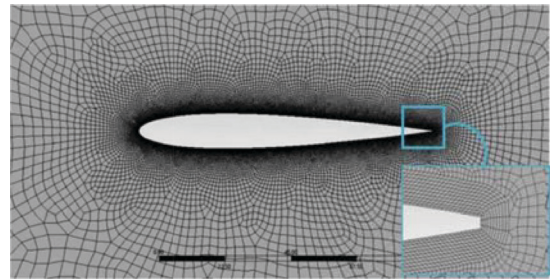


Figure 4. Mesh detail

### 2.3 METHOD VALIDATION

To ensure the accuracy of the calculation results, the Grid Convergence Index (GCI) method is used for grid convergence analysis, which is first proposed by Roache [14] and has since undergone extensive researches and modifications. The methodology proposed by Celik et al. [15] is used for the GCI method in the present study. In this approach, the refinement factor ( $r$ ) is defined as;

$$r_{21} = \frac{h_2}{h_1} \quad (10)$$

$$r_{32} = \frac{h_3}{h_2} \quad (11)$$

where  $h_1$ ,  $h_2$ , and  $h_3$  are the sizes of the successive grids. The subscripts 1, 2, and 3 represent fine, medium, and coarse grids, respectively.

Celik et al. [15] recommended that the grid refinement ratio be greater than 1.3. Therefore, the grid refinement ratio is set to  $r = \sqrt{2}$ .  $\varphi_1$ , and  $\varphi_2$  and  $\varphi_3$  represent the solutions of the fine, medium and coarse grids, respectively. The convergence ratio ( $R$ ) can be derived by dividing medium-fine and coarse-medium approaches.

$$R = \frac{\varphi_2 - \varphi_1}{\varphi_3 - \varphi_2} \tag{12}$$

1. Monotonic convergence:  $0 < R < 1$ ,
2. Oscillatory convergence:  $R < 0$ ,
3. Divergence:  $R > 1$ .

Firstly, the method p, q and s are defined as:

$$p = \frac{1}{\ln r_{21}} \left| \ln \left| \frac{\varepsilon_{32}}{\varepsilon_{21}} \right| + q(p) \right| \tag{13}$$

$$q_{(p)} = \ln \left( \frac{r_{21}^p - s}{r_{32}^p - s} \right) \tag{14}$$

$$s = 1 \bullet \operatorname{sgn} \left( \frac{\varepsilon_{32}}{\varepsilon_{21}} \right) \tag{15}$$

And  $\varepsilon_{ij}$  is defined  $\varepsilon_{ij} = \varphi_i - \varphi_j$  ;

Extrapolated values are defined by the following equation:

$$\varphi_{ext}^{21} = \frac{r_{21}^p \varphi_1 - \varphi_2}{r_{21}^p - 1} \tag{16}$$

The approximate relative error is calculated as follows:

$$e_a^{21} = \left| \frac{\varphi_1 - \varphi_2}{\varphi_1} \right| \tag{17}$$

The extrapolated relative error is defined as:

$$e_{ext}^{21} = \left| \frac{\varphi_{ext}^{21} - \varphi_1}{\varphi_{ext}^{21}} \right| \tag{18}$$

Finally, the fine-grid convergence index can be calculated with the equation:

$$GCI = \frac{1.25 e_a^{21}}{r_{21}^p - 1} \tag{19}$$

Three grids, namely fine grid (268185), medium (188110), and coarse grid (755980), are generated. The cases for

the motion parameter group ( $h_0 = c$ ,  $\theta_0 = 15^\circ$ ,  $\varphi = 75^\circ$ ) are selected for calculations. The force parameters  $C_t$ ,  $C_l$  and  $C_m$  are used as the indicators for GCI analysis. The results of grid convergence analysis are given in Table 2, in which the results are average values in time domain. For different force parameters,  $R$  is less than 0 which belongs to oscillation convergence, and GCI is less than 6%. This indicates that the impact of the grid change is accepted to be small between the fine grid and medium grid, and the satisfactory grid convergence is obtained.

Table 2-1. Results of grid convergence analysis

	$\varphi_1$	$\varphi_2$	$\varphi_3$
$C_t$	1.067	1.077	1.062
$C_l$	-0.393	-0.399	-0.350
$C_m$	-0.139	-0.142	-0.138

Table 2-2. Results of grid convergence analysis

	$R$	$e_a^{21}$	$GCI$
$C_t$	-0.6923	0.01015	0.0306
$C_l$	-0.1343	0.01692	0.0511
$C_m$	-0.5613	0.01638	0.04943

For a further understanding of the accuracy of the numerical method, the hydrodynamic performance of the flapping hydrofoil for the motion parameter group ( $h_0 = 0.75c$ ,  $\theta_0 = 23^\circ$ ,  $\varphi = 75^\circ$ ) is calculated using the medium grid strategy, and the result is compared with that of Chen et al. [11]. The thrusts of current method and Chen are shown in Table 3. The result of current method just has a difference of 3.85% compared with that of Chen. Therefore, the median grid strategy is used for further investigations.

Table 3. Thrusts of current method and Chen et al. [11]

	$C_t$
Result of Chen	0.5662
Result of current method	0.5444

### 3. NUMERICAL SIMULATION RESULTS AND DISCUSSION

#### 3.1 INFLUENCE OF MOTION PARAMETERS ON THRUST PULSATION AMPLITUDE

There are two main sources of flapping wing thrust:

1. The motion of the flapping hydrofoil disrupts the flow field, creating a pressure difference between the upper and lower surfaces of the hydrofoil. This

pressure difference generates thrust in the horizontal direction.

- The flapping hydrofoil movement generates an anti-Karman vortex street, which in turn produces a thrust [16]. The combination of the leading-edge and trailing edge vortices will affect the strength of the vortex, and thus affect the thrust in further.

Figure 5 illustrates the cloud diagram of the average values of thrust varying with motion parameters for each numerical simulation group in this study. The thrust of the flapping hydrofoil presents a cyclical fluctuation, and the pulsation amplitude of thrust not only impacts the stability of propulsion performance but also affects the vibration and noise performance. The effects of the heave amplitude, the pitch amplitude as well as the phase difference between heave and horizontal motions on the thrust pulsation amplitude are investigated in detail.

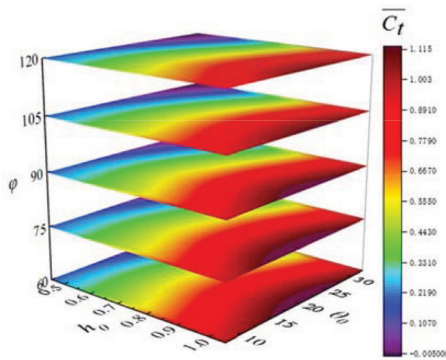


Figure 5. Contours of thrust pulsation amplitude under different motion parameters

### 3.1(a) Effect of Heave Amplitude on Thrust Pulsation Amplitude

To reveal the effect of heave amplitude on the thrust pulsation amplitude of flapping hydrofoil, the thrusts of the flapping hydrofoil with different heave amplitudes are obtained at  $\theta_0 = 25^\circ$  and  $\varphi = 90^\circ$ , as shown in the figure 6, in which  $T$  denotes the time for one cycle.

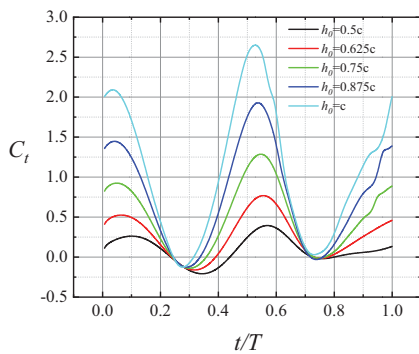


Figure 6. Thrusts for different heave amplitudes over time in one cycle ( $\theta_0 = 25^\circ$ ,  $\varphi = 90^\circ$ ).

It can be observed that the change in the heave amplitude impacts the rate of change in thrust as well as the maximum thrusts. While the heave amplitude has little effect on the minimum thrust value. The results indicate that the effect of heave amplitude on thrust pulsation amplitude mainly involves the alteration of the maximum thrust value. Selecting a larger heave amplitude is of great advantage for enhancing thrust. On the other hand, heave amplitude significantly affects  $P_a$ , resulting in a larger thrust pulse.

To have a deep understanding about the flow field characteristics around the flapping hydrofoil, Figure 7 shows the pressure contours of the flapping hydrofoil with different heave amplitudes at  $t = 0.444T$ . The results demonstrate that the alterations to the heave amplitude has a remarkable effect on the pressure distribution on the upper and lower surfaces of the flapping hydrofoil. Under constant conditions in both  $\theta$  and  $\varphi$ , the greater the amplitude, the greater the pressure difference. This, in turn, causes the changes of the pressure difference between the upper and lower surfaces, resulting in a variation in the magnitude of the thrust generated.

### 3.1(b) Effect of Pitch Amplitude on Thrust Pulsation Amplitude

The effect of pitch amplitude on the thrust pulsation amplitude of flapping hydrofoil is studied in this section. Firstly, the thrusts of the flapping hydrofoil for different pitch amplitudes at  $h_0 = 0.5c$  and  $\varphi = 90^\circ$  are analyzed, and the thrusts for different pitch amplitudes over time in one cycle are shown in Figure 8. Table 4 gives the corresponding maximum and minimum thrust values and the thrust pulsation amplitude. It can be seen that, different from the effect of heave amplitude on thrust, the pitch amplitude not only affects the maximum value of thrust, but also changes the minimum value.

Both the maximum and minimum thrusts gradually decrease, but the thrust pulsation coefficient first decreases and then increases, with the increase of pitch amplitude. It shows that the pitch amplitude interacts with the thrust pulsation at certain rise value and phase angle. If the pitch amplitude is improperly set when designing motion parameters, the thrust pulsation amplitude will be increased, and the vibration may be exacerbated.

The propulsion performance of the flapping hydrofoil at  $h_0 = 0.75c$  and  $\varphi = 90^\circ$  is also simulated, and the results are shown in Figure 9 and Table 5. By comparing Figure 8 and Figure 9, it can be found that the effect of the pitch amplitude on the thrust pulsation amplitude and the average value of thrust gets more obvious at smaller heave amplitude. Therefore, the impact of pitch amplitude on the thrust pulsation amplitude is affected by the heave amplitude. In the analysis of thrust pulsation amplitude, the interaction effect between the pitch and heave amplitudes should be considered.

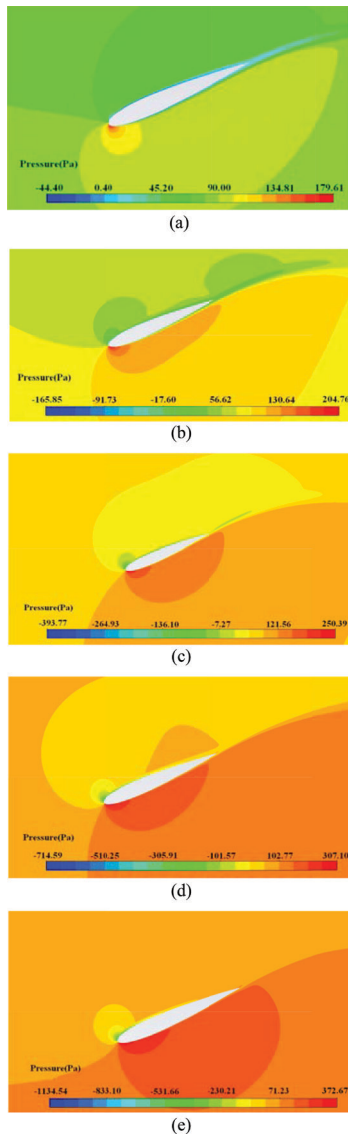


Figure 7. Pressure contours of flapping hydrofoil for different heave amplitudes at  $t = 0.444T$  ( $\theta_0 = 25^\circ$ ,  $\varphi = 90^\circ$ ). (a)  $h_0 = 0.5c$ , (b)  $h_0 = 0.625c$ , (c)  $h_0 = 0.75c$ , (d)  $h_0 = 0.875c$ , (e)  $h_0 = c$ .

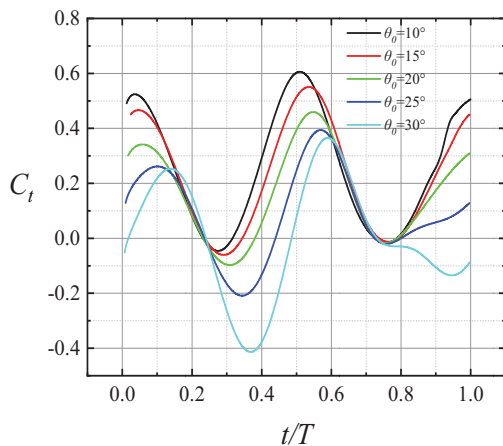


Figure 8. Thrusts for different pitch amplitudes over time in one cycle ( $h_0 = 0.5c$ ,  $\varphi = 90^\circ$ ).

Table 4. Maximum and minimum thrust values at  $h_0 = 0.5c$  and  $\varphi = 90^\circ$

	Maximum	Minimum	$P_a$
$\theta_0 = 10^\circ$	0.606	-0.045	0.651
$\theta_0 = 15^\circ$	0.551	-0.060	0.611
$\theta_0 = 20^\circ$	0.459	-0.097	0.556
$\theta_0 = 25^\circ$	0.390	-0.208	0.598
$\theta_0 = 30^\circ$	0.367	-0.413	0.780

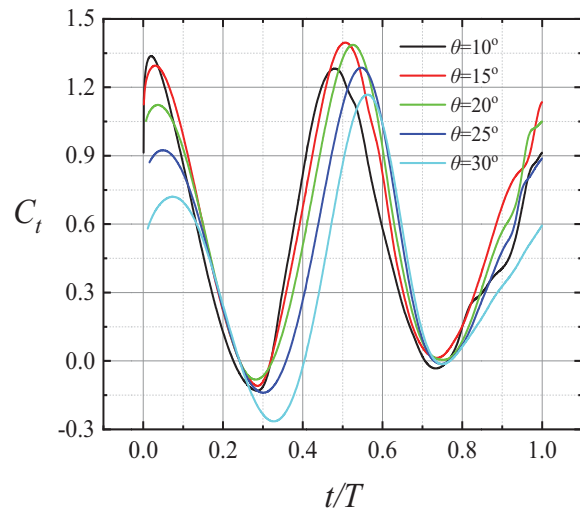


Figure 9. Thrusts for different pitch amplitudes over time in one cycle ( $h_0 = 0.75c$ ,  $\varphi = 90^\circ$ ).

Table 5. Maximum and minimum thrust values at  $h_0 = 0.75c$  and  $\varphi = 90^\circ$

	Maximum	Minimum	$P_a$
$\theta_0 = 10^\circ$	1.282	-0.130	1.412
$\theta_0 = 15^\circ$	1.390	-0.109	1.499
$\theta_0 = 20^\circ$	1.380	-0.081	1.461
$\theta_0 = 25^\circ$	1.284	-0.139	1.419
$\theta_0 = 30^\circ$	1.164	-0.268	1.432

Figure 10 shows the pressure contours of the flapping hydrofoil for different pitch amplitudes at  $t = 0.444T$  when  $h_0 = 0.75c$  and  $\varphi = 90^\circ$ . The results demonstrate that the pitch amplitude has a remarkable effect on the pressure distribution around the flapping hydrofoil. The pressure value around the hydrofoil in general decreases gradually as the pitch amplitude increases. The high pressure region near the lower surface contracts gradually from the downstream to the leading edge of hydrofoil, while the low pressure region near the upper surface extends downstream with the increase of pitch amplitude. The pressure difference between the upper and lower surfaces decreases gradually as the pitch amplitude increases at  $t = 0.444T$ . Therefore, the thrust shows a decreasing tendency with the increase of pitch amplitude.

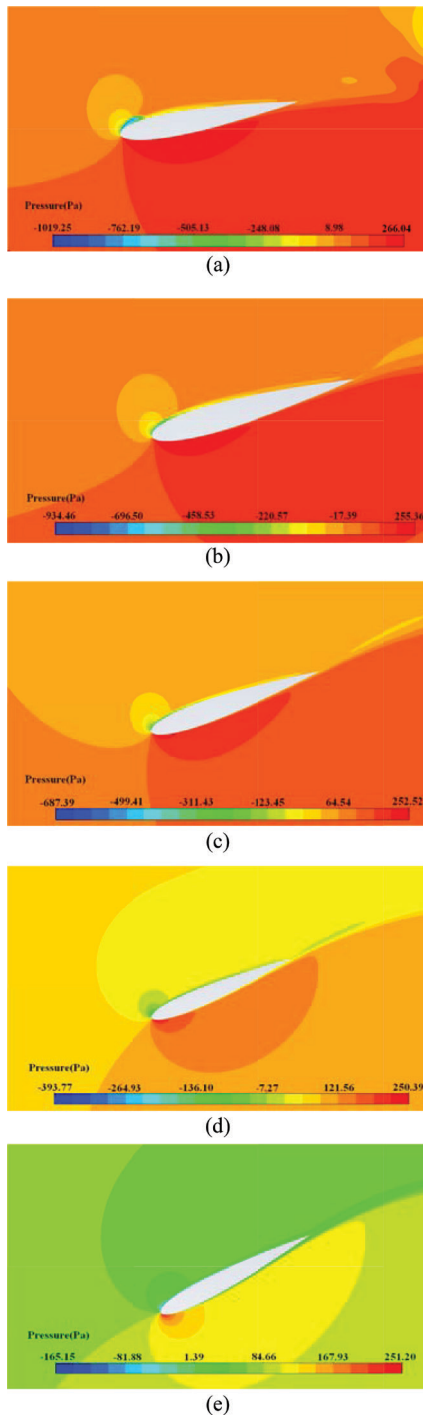


Figure 10. Pressure contours of flapping hydrofoil for different pitch amplitudes ( $h_0 = 0.75c$ ,  $\varphi = 90^\circ$ ,  $t = 0.444T$ ). (a)  $\theta_0 = 10^\circ$ , (b)  $\theta_0 = 15^\circ$ , (c)  $\theta_0 = 20^\circ$ , (d)  $\theta_0 = 25^\circ$ , (e)  $\theta_0 = 30^\circ$ .

### 3.1(c) Effect of Heave and Horizontal Motion Phase Difference on Thrust Pulsation Amplitude

The effect of the phase difference between heave and horizontal motions on the thrust pulsation amplitude is investigation in further. The thrusts of the flapping hydrofoil for different pitch amplitudes ranging from  $60^\circ$  to  $120^\circ$  at  $h_0 = 0.5c$ ,  $\theta_0 = 30^\circ$  and  $h_0 = 0.875c$ ,  $\theta_0 = 30^\circ$

are analyzed respectively, and the thrusts over time in one cycle are shown in Figure 11 and Figure 12, respectively. Table 6 and Table 7 give the corresponding maximum and minimum thrust values and the thrust pulsation amplitudes.

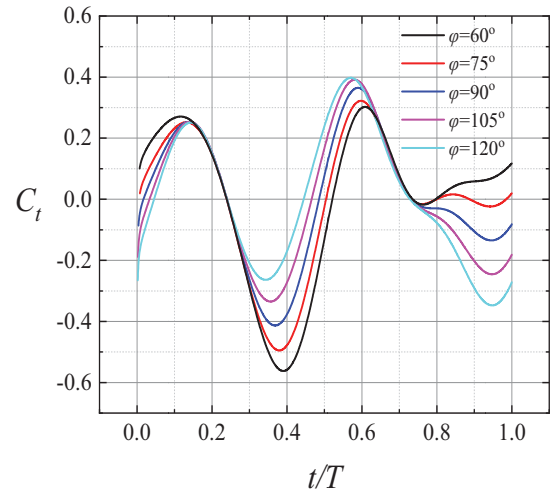


Figure 11. Thrusts for different phase differences between heave and horizontal motions over time in one cycle ( $h_0 = 0.5c$ ,  $\theta_0 = 30^\circ$ ).

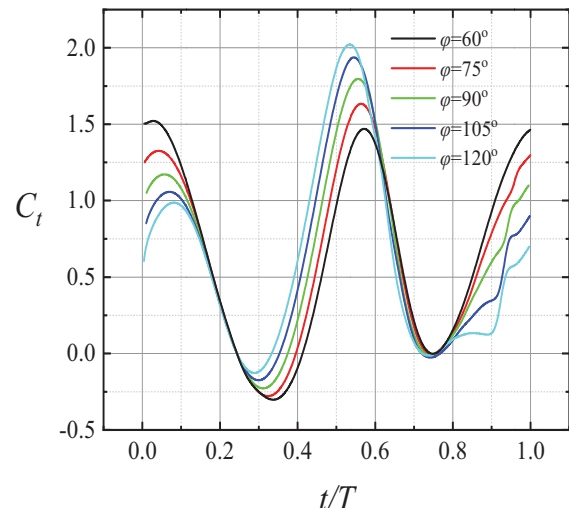


Figure 12. Thrusts for different phase differences between heave and horizontal motions over time in one cycle ( $h_0 = 0.875c$ ,  $\theta_0 = 30^\circ$ ).

Table 6. Maximum and minimum thrust values at  $h_0 = 0.5c$  and  $\theta_0 = 30^\circ$

	Maximum	Minimum	$P_a$
$\varphi = 60^\circ$	0.300	-0.560	0.860
$\varphi = 75^\circ$	0.323	-0.490	0.813
$\varphi = 90^\circ$	0.363	-0.410	0.773
$\varphi = 105^\circ$	0.386	-0.335	0.721
$\varphi = 120^\circ$	0.398	-0.260	0.658

Table 7. Maximum and minimum thrust values at  $h_0 = 0.875c$  and  $\theta_0 = 30^\circ$ .

	Maximum	Minimum	$P_a$
$\varphi = 60^\circ$	1.465	-0.309	1.765
$\varphi = 75^\circ$	1.624	-0.285	1.909
$\varphi = 90^\circ$	1.800	-0.235	2.035
$\varphi = 105^\circ$	1.931	-0.174	2.105
$\varphi = 120^\circ$	2.016	-0.137	2.153

For the cases that  $h_0 = 0.5c$  and  $\theta_0 = 30^\circ$ , both the thrust maximum and the minimum values increase, but the thrust pulsation amplitude decreases gradually, with the increase of phase difference. The effect of the phase difference on the thrust at about  $t = 0.22T$  and  $t = 0.68T$  can be neglected. When the heave amplitude  $h_0$  is  $0.875c$ , as shown Figure 12 and Table 7, the maximum and the minimum values of thrust also increase as the phase difference increases, while the thrust pulsation amplitude shows an increasing trend.

Therefore, the effect of phase difference on the thrust pulse amplitude is also affected by the heave amplitude.

Figure 13 shows the pressure contours of the flapping hydrofoil for different phase differences at  $t = 0.444T$  when  $h_0 = 0.875c$  and  $\theta_0 = 30^\circ$ . The pressure value around the hydrofoil in general increases gradually as the phase difference increases. The high pressure region near the lower surface extends downstream dramatically with the increase of phase difference, and the pressure difference between the upper and lower surfaces increases gradually as the phase difference increases at  $t = 0.444T$ . Therefore, the thrust shows an increasing tendency with the increase of phase difference.

### 3.2 INTERACTION OF MOTION PARAMETERS

The above analysis of the effects of the heave amplitude, the pitch amplitude as well as the phase difference between heave and horizontal motions on the thrust and its pulsation amplitude shows that the interaction effects among the motion parameters should be considered. The fitting function between the thrust pulse amplitude and the motion parameters is established, and the effect of each item on the thrust pulsation amplitude is quantified by the coefficient term of the fitting function.

In this study, the interaction effect refers to the effects of the pitch amplitude and the phase difference between heave and horizontal motions on the thrust pulsation amplitude depending on different levels of heave amplitude.

The Levenberg-Marquardt algorithm is a combination of the gradient descent method and the Gauss-Newton method, not only retains the control of local characteristics

of the Gauss-Newton method, but also has the global characteristics of the gradient method. It is obviously better than the conjugate gradient method and BP (Back Propagation) algorithm with variable learning rate in terms of training time and accuracy. [17, 18]

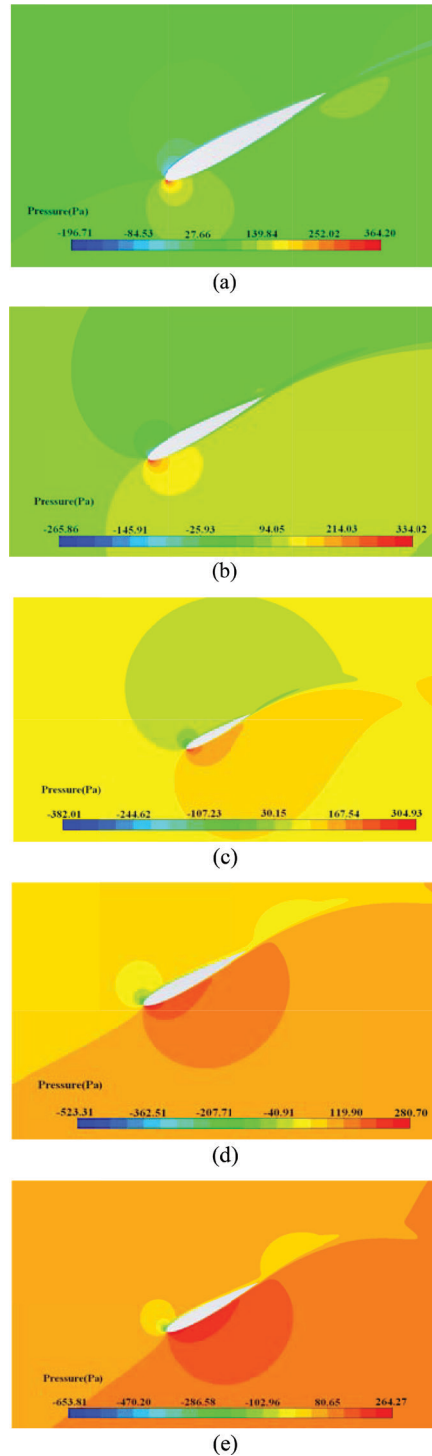


Figure 13. Pressure contours of flapping hydrofoil for different phase differences between heave and horizontal motions ( $h_0 = 0.875c$ ,  $\theta_0 = 30^\circ$ ,  $t = 0.444T$ ). (a)  $\varphi = 60^\circ$ , (b)  $\varphi = 75^\circ$ , (c)  $\varphi = 90^\circ$ , (d)  $\varphi = 105^\circ$ , (e)  $\varphi = 120^\circ$

This study uses the Levenberg-Marquardt optimization algorithm to perform function fitting analysis on the three motion parameters and the thrust pulsation amplitude. Given nonlinear fitting function relation:

$$y = bx_1 + c_2x_2 + dx_3 + ex_1x_2 + fx_1x_3 + gx_2x_3 + hx_1x_2x_3 + a \quad (20)$$

where  $x_1, x_2,$  and  $x_3,$  represent the phase difference between heave and horizontal motions, the heave amplitude and the pitch amplitude, respectively.

In polynomial fitting, the  $R_2$  value is a very important indicator that can be used to assess the degree of fit of the fitted curve. The  $R_2$  value is a numerical value between -1 and 1, which represents the correlation between the fitted curve and the actual data. When the  $R_2$  value is 1, it means that the fit curve completely coincides with the actual data, and the fit degree is very good; when the  $R_2$  value is 0, there is no correlation between the fit curve and the actual data, and the fit degree is very poor; when the  $R_2$  value is -1, there is a completely opposite correlation between the fit curve and the actual data, and the fit degree is very poor.  $R_2$  is 0.94611 after function fitting, indicating a good degree of function fitting. The fitting function coefficients are shown in Table 8:

Table 8. Fitted function coefficients

Parameters	Value
a	1
b	-0.02948
c	1.9317
d	-0.13733
e	0.02697
f	0.00153
g	0.13853
h	-0.00155

According to the coefficient values in the function fitting relation, it can be seen that the heave amplitude has the greatest effect on the thrust pulsation amplitude, followed by the pitch amplitude. The phase difference between horizontal and heave motions has the least effect. In addition, the observation of cross term  $x_2x_3$  coefficient and pitch amplitude coefficient proves that the impact of the pitch amplitude on the thrust pulsation amplitude is affected by the level of heave amplitude, and there is an obvious interactive effect between the pitch amplitude and the heave amplitude. The phase difference between horizontal and heave motions is also affected by the level of heave amplitude.

#### 4. CONCLUSIONS

In this paper, the effects of motion parameters of elliptical trajectory of a flapping hydrofoil on the thrust pulsation

amplitude are studied, and some conclusions can be concluded as follows:

1. The grid convergence analysis is carried out to validate the grid generating strategy and numerical method. The optimal grid generating strategy has been identified, and the simulated result is in a good agreement with existing work.
2. The heave amplitude is positive correlation with the thrust pulsation amplitude, and mainly affects the maximum value of thrust, but has a marginal effect on the minimum value.
3. Different from the heave amplitude, the pitch amplitude not only affects the maximum value of thrust, but also changes the minimum value. The effect of the pitch amplitude on the thrust pulsation amplitude and the average value of thrust gets more obvious at smaller heave amplitude.
4. There is an obvious interaction among the pitch amplitude, the heave amplitude and the phase difference between heave and horizontal motions. The effects of the three motion parameters on the thrust pulsation amplitude are analyzed through function fitting analysis, and the effect degrees of different motion parameters are revealed in further.

Due to a large amount of calculations, the numerical study about the effects of full motion parameters on the thrust of the flapping hydrofoil is not completed, and the function fitting of the full parameters on the thrust of the flapping hydrofoil is not realized. In the future, the numerical simulation of the full motion parameters can be carried out, so as to serve as a basis for the design of motion trajectory and optimization of flapping hydrofoil.

#### 5. ACKNOWLEDGEMENTS

This research is financially supported by the Liaoning Provincial Natural Science Foundation of China (Grant No. LJKMZ20220367) and the Fundamental Research Funds for the Central Universities (3132023121).

#### 6. REFERENCES

1. DING, H. (2015). *Research on propulsion characteristics and motion performance of bionic flapping-wing underwater vehicle*, Ph.D. Thesis, Northwestern Polytechnical University, CN.
2. TECHET, A. H. (2008). *Propulsive performance of biologically inspired flapping foils at high Reynolds numbers*. J Exp Biol., 211(Pt 2): 274–9.
3. ASHRAF, M. A., et al. (2011). *Reynolds number, thickness and camber effects on flapping airfoil propulsion* [J]. Journal of Fluids and Structures. 27(2): 145–60.

4. READ, D. A., et al. (2003). *Forces on oscillating foils for propulsion and maneuvering*. Journal of Fluids and Structures. 17(1): 163–83.
5. YU, D., et al. (2017). *Numerical study of the effect of motion parameters on propulsive efficiency for an oscillating airfoil*. Journal of Fluids and Structures. 68: 245–63.
6. ZHANG, J. Z., et al. (2015). *Effects of local oscillation of airfoil surface on lift enhancement at low Reynolds number*. Journal of Fluids and Structures. 57: 49–65.
7. QADRI, M. N. M., ZHAO, F. W., TANG, H. (2020). *Fluid-structure interaction of a fully passive flapping foil for flow energy extraction*. International Journal of Mechanical Sciences. 177: 105587.
8. ESFAHANI, J. A., et al. (2015). *Fluid structures of flapping airfoil with elliptical motion trajectory*. Computers & Fluids. 108: 142–55.
9. YANG, S, et al. (2017). *Effect of motion trajectory on the aerodynamic performance of a flapping airfoil*. Journal of Fluids and Structures. 75: 213–32.
10. ZHANG, Y., YANG, F., WANG, D., JIANG, X. (2021). *Numerical investigation of a new three-degree-of-freedom motion trajectory on propulsion performance of flapping foils for UUVs*. Ocean Engineering, 224(4): 108763.
11. CHEN, X., et al. (2018). *Numerical investigation of elliptical motion on propulsion performance of a flapping hydrofoil*. Proceedings of the 2018 OCEANS-MTS/IEEE Kobe Techno-Ocean (OTO), F, [C].
12. QING, X. and QIANG, Z. (2014). *A review on flow energy harvesters based on flapping foils*. Fluid Struct. 46: 174–191.
13. Roache, P. J., (1998) *Verification of codes and calculations*. AIAA J. 36(5): 696–702.
14. Celik, I. B., et al. (2008). *Procedure for estimation and reporting of uncertainty due to discretization in CFD applications*. J. Fluids Eng. Trans. ASME.130 (7): 0780011–0780014.
15. YOUNG, J. (2005). *Numerical Simulation of the unsteady aerodynamics of flapping airfoils*, Ph.D. Thesis, University of New South Wales, Sydney, Australia.
16. LI, F., et al. (2021). *Influence of wavy leading edge on hydrofoil turbulent interference noise*. Journal of Northwestern Polytechnical University. 39(06): 1266–73.
17. ZHAO, H., et al. (2002). *Neural network supervisory control based on Levenberg-Marquardt algorithm*. Journal of Xi'an Jiaotong University. (05): 523–7.
18. ZHANG, H. Y. and GEN, Z. (2009). *A new interpretation of the Levenberg-Marquardt algorithm*. Computer Engineering and Applications. 45(19): 5–8.